

Exploiting Directionality for Millimeter-Wave Wireless System Improvement

George R. MacCartney Jr., Mathew K. Samimi, and Theodore S. Rappaport

NYU WIRELESS

NYU Polytechnic School of Engineering

Brooklyn, NY 11201

{gmac,mks,tsr}@nyu.edu

Abstract—This paper presents directional and omnidirectional RMS delay spread statistics obtained from 28 GHz and 73 GHz ultrawideband propagation measurements carried out in New York City using a 400 Megachips per second broadband sliding correlator channel sounder and highly directional steerable horn antennas. The 28 GHz measurements did not systematically seek the optimum antenna pointing angles and resulted in 33% outage for 39 T-R separation distances within 200 m. The 73 GHz measurements systematically found the best antenna pointing angles and resulted in 14.3% outage for 35 T-R separation distances within 200 m, all for mobile height receivers. Pointing the antennas to yield the strongest received power is shown to significantly reduce RMS delay spreads in line-of-sight (LOS) environments. A new term, *distance extension exponent (DEE)* is defined, and used to mathematically describe the increase in coverage distance that results by combining beams from angles with the strongest received power at a given location. These results suggest that employing directionality in millimeter-wave communications systems will reduce inter-symbol interference, improve link margin at cell edges, and enhance overall system performance.

Index Terms—mmWave; 5G; 28 GHz; 73 GHz; RMS delay spread; distance extension; omnidirectional models; multipath;

I. INTRODUCTION

The growing demand for wireless broadband communications has led to the exploration of the underutilized millimeter-wave (mmWave) spectrum where a vast amount of raw bandwidth can be exploited to provide multi-gigabit per second data rates for backhaul, fronthaul, and mobile applications [1]. Highly directional horn antennas at the transmitter (TX) and receiver (RX) make up for the additional free space path loss induced by the order of increase in carrier frequency, resulting in many more directional systems than at today's Microwave and Ultra-High Frequency (UHF) bands below 6 GHz, where quasi-omnidirectional antennas are commonplace [2]. Recent outdoor mmWave measurements using less than 1 W of transmit power have shown that future cell radii will be 200 m or so, implying that at such short distances, atmospheric and

TABLE I: T-R separation distances and number of TX-RX location combinations where signal was detected, and where outages occurred, for LOS and NLOS environments at 28 GHz (2012) and 73 GHz in Manhattan (2013). Note that the 28 GHz campaign did not systematically search for pointing angles between the TX and RX antennas to make a link, but the 73 GHz campaign did.

Manhattan Measurements ¹			
		28 GHz TX/RX: 10.9° HPBW	73 GHz TX/RX: 7° HPBW
# of locations measured ($d \leq 200$ m)	LOS	6	5
	NLOS	33	30
# of locations measured for all d	LOS	6	5
	NLOS	68	31
# of locations with signal ($d \leq 200$ m)	LOS	6 (31 m $\leq d \leq$ 102 m)	5 (30 m $\leq d \leq$ 54 m)
	NLOS	20 (61 m $\leq d \leq$ 187 m)	25 (48 m $\leq d \leq$ 190 m)
# of outage locations ($d \leq 200$ m)	LOS	0	0
	NLOS	13 (96 m $\leq d \leq$ 193 m)	5 (168 m $\leq d \leq$ 198 m)
# of locations with signal for all d	LOS	6 (31 m $\leq d \leq$ 102 m)	5 (30 m $\leq d \leq$ 54 m)
	NLOS	20 (61 m $\leq d \leq$ 187 m)	25 (48 m $\leq d \leq$ 190 m)
# of outage locations for all d	LOS	0	0
	NLOS	48 (96 m $\leq d \leq$ 425 m)	6 (168 m $\leq d \leq$ 216 m)

rain attenuations will not be a major concern for mmWave outdoor urban-microcell (UMi) propagation [4].

Future mmWave radio-systems must be designed appropriately with the help of statistical channel models (SCM), such as the widespread 3GPP and WINNER II models that were used to characterize the sub-6 GHz wireless channel [5]. Recent mmWave propagation measurements, have faithfully accounted for mmWave wideband channel properties, with new statistical directional and omnidirectional path loss models, and temporal and spatial channel models [6]–[11].

The time dispersive characteristics of mmWave wideband channels have, however, received little attention to date. The omnidirectional root-mean-square (RMS) delay spread pro-

¹Three additional measurement studies in 2012 at 28 GHz were conducted in Manhattan and Brooklyn but are not considered for this study since the scenarios were different, including: (1) 28 GHz measurements with a narrowbeam TX antenna (10.9° HPBW) and widebeam RX antennas (28.8° HPBW) were conducted for 5 RX locations in Manhattan. (2) 28 GHz measurements with narrowbeam TX and RX antennas (10.9° HPBW) were conducted for 5 RX locations in Brooklyn. (3) 28 GHz measurements with a widebeam TX antenna (28.8° HPBW) and narrowbeam RX antennas (10.9° HPBW) were conducted for 4 RX locations in Brooklyn [3].

TABLE II: Broadband sliding correlator channel sounder system specifications used to conduct the 28 GHz and 73 GHz dense UMi propagation measurements in New York City [6].

Manhattan Measurements		
Campaign	28 GHz (2012)	73 GHz (2013)
TX / RX IF Frequency	5.4 GHz	5.625 GHz
TX / RX LO Frequency	22.6 GHz	67.875 GHz
TX / RX PN Chip Rate	400 Mcps / 399.95 Mcps	
RF Bandwidth (Null-to-null)	800 MHz	
Multipath Time Resolution	2.5 ns	
Max. TX RF Power	30 dBm	14.6 dBm
Max. Measurable Path Loss (5 dB SNR)	178 dB	181 dB
TX / RX Antenna Polarization	Vertical	
TX / RX Antenna Gain	24.5 dBi	27 dBi
TX / RX Az. HPBW	10.9°	7°
TX / RX El. HPBW	8.6°	7°
TX Antenna Heights	7 and 17 m	
RX Antenna Heights	1.5 m	2 m

vides an important measure of channel time dispersion and multipath, and greatly impacts equalization, cyclic-prefixes, and receiver architectures when designing UWB systems. Multipath components (MPCs) arise from propagating signals that experience reflection and scattering, and cause inter-symbol interference (ISI). The measured RMS delay spread thus provides valuable channel knowledge. Omnidirectional RMS delay spreads were extensively measured for the UHF/Microwave bands in order to design current 3G and 4G systems, resulting in RMS delay spreads from 15.7 ns to 23.75 ns with an UWB pulse of 2.2 GHz between 3.1 and 5.3 GHz [12]. Typical mean RMS delay spreads at 400 MHz and 1900 MHz in multipath-rich LOS and NLOS environments were measured on the order of 300-400 ns and 730 ns, respectively, over 10-20 MHz of RF bandwidth [13], [14]. The mean and maximum RMS delay spreads observed using directional antennas in a NLOS dense urban wideband cellular study were 12.2 ns and 117 ns at 38 GHz, respectively [7]. 90% of 59 GHz collected wideband measurements had RMS delay spreads less than 20 ns in a dense UMi environment for T-R separation distances less than 200 m [15], and the typical RMS delay spread in another study in a city street environment was below 20 ns [16].

28 GHz and 73 GHz mmWave UWB propagation measurements in New York City were collected with a 400 Megachips per second (Mcps) broadband sliding correlator channel sounder, each with a pair of highly directional steerable horn antennas used at the TX and RX, for 74 and 36 TX-RX location combinations at 28 GHz and 73 GHz, respectively, for mobile RX heights [4], [6]. Power delay profiles (PDPs) were measured at unique azimuth and elevation antenna pointing angles at the TX and RX, allowing us to model both temporal and spatial channel characteristics. Table I lists the number of LOS and NLOS locations measured

and the range of distances for both 28 GHz and 73 GHz LOS and NLOS environments in Manhattan, where signal was detected and where outages occurred. High-gain directional antennas were used to complete mmWave links in order to make up for the increase in free space path loss at higher frequencies compared to today's bands. MmWave channels must therefore be characterized using directional statistical models obtained from unique pointing angle narrowbeam measurements, as reported in [4], [6], [17]. In this paper, we present both directional and omnidirectional RMS delay spread statistics based on our 28 GHz and 73 GHz propagation measurements, that can be used in developing beam combining and beamforming algorithms to be used in future electrically-steered on-chip antennas [18].

Section II presents directional RMS delay spreads obtained from all pointing angle measurements between the TX and RX, Section III introduces a new term, the *distance extension exponent* (DEE), used to determine distance extension when combining beams from unique pointing angles with the strongest received power, Section IV gives omnidirectional RMS delay spreads synthesized from absolute timing power delay profiles recovered using 3-D ray-tracing techniques, and Section V concludes the paper.

II. DIRECTIONAL RMS DELAY SPREAD

UWB propagation measurement campaigns were performed in 2012 and 2013 in dense urban LOS and NLOS environments to assess the viability of mmWave outdoor communications. 400 Mcps broadband sliding correlator channel sounders at 28 and 73 GHz shared a similar architecture but with different IF, LO, and RF up- and down-conversion front-ends. T-R separation distances ranged from 30 m to 425 m, where several thousands of PDPs were recorded at many different azimuth and elevation pointing angle combinations using steerable high-gain horn antennas (10.9° (at 28 GHz) and 7° (at 73 GHz), half-power beamwidth (HPBW)) at both the TX and RX, providing maximum measurable path loss of 178 dB and 181 dB at 28 GHz and 73 GHz, respectively. Although both backhaul (4.06 m) and mobile (2 m) RX heights were measured at 73 GHz, only mobile measurements are considered in this paper for proper comparison with the 28 GHz mobile (1.5 m) measurements.

The 28 GHz measurements were more rigid, in that they did not systematically point and search for antenna pointing angles between the TX and RX that resulted in the strongest power, whereas the 73 GHz measurement campaign did search for TX and RX antenna pointing angles that resulted in links with the strongest received power. At both 28 and 73 GHz, omnidirectional path loss models were created by summing PDPs from adjacent and orthogonal antenna beams so as to not double count overlapping angles or multipath energy. While the 73 GHz measurements scanned a larger portion of the 4π steradian sphere, both measurements resulted in consistent path loss models [8]. The measurement equipment specifications are listed in Table II, and additional details are available in [4], [6].

TABLE III: LOS and NLOS mean RMS delay spreads and standard deviations in New York City at 28 GHz and 73 GHz over all arbitrary directional antenna pointing angles in the azimuth and elevation planes for all locations with detectable signal.

Directional RMS Delay Spread for Locations with Signal Over All Pointing Angles and Distances Between the TX and RX	LOS		NLOS	
	μ (ns)	σ (ns)	μ (ns)	σ (ns)
28 GHz (10.9° HPBW)	28.8	44.3	17.4	28.3
73 GHz (7° HPBW)	13.9	22.0	11.1	22.9

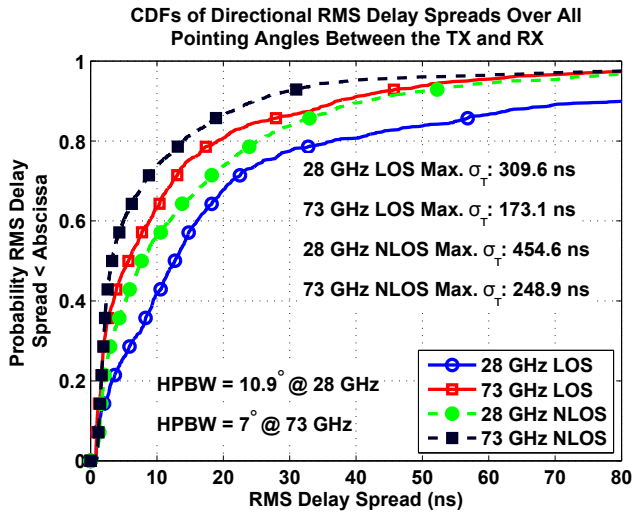


Fig. 1: 28 GHz and 73 GHz LOS and NLOS RMS delay spread CDFs over all pointing angles in the azimuth and elevation planes in New York City using high-gain directional antennas (HPBW of 10.9° at 28 GHz and 7° at 73 GHz). 28 GHz RMS delay spreads are larger than 73 GHz RMS delay spreads in both LOS and NLOS environments.

Fig. 1 shows cumulative distribution functions (CDFs) of the LOS and NLOS directional RMS delay spreads at 28 GHz and 73 GHz over all pointing angles between the TX and RX antennas, where RMS delay spreads $\sigma_\tau(\theta_i, \phi_j)$ at a given azimuth angle θ_i and elevation angle ϕ_j combination were computed from Eqs. (1) to (3) [2]:

$$\bar{\tau}(\theta_i, \phi_j) = \frac{\sum_k P(\tau_k, \theta_i, \phi_j) \tau_k}{\sum_k P(\tau_k, \theta_i, \phi_j)} \quad (1)$$

$$\overline{\tau^2}(\theta_i, \phi_j) = \frac{\sum_k P(\tau_k, \theta_i, \phi_j) \tau_k^2}{\sum_k P(\tau_k, \theta_i, \phi_j)} \quad (2)$$

$$\sigma_\tau(\theta_i, \phi_j) = \sqrt{\overline{\tau^2} - (\bar{\tau})^2} \quad (3)$$

where $P(\tau_k, \theta_i, \phi_j)$ is the relative amplitude of multipath in mW/ns in time bin τ_k , for a measured azimuth angle θ_i and elevation angle ϕ_j direction. In our work, each directional PDP measurement was processed using a 5 dB above mean thermal noise floor SNR threshold, where all measured signals above this threshold were deemed valid and all signal levels below were ignored. Directional LOS RMS delay spreads over all arbitrary pointing angles are for RX locations where the TX

and RX were in clear LOS of each other, with the TX and RX antennas aligned on boresight, but also when TX and RX antennas were not necessarily aligned on boresight, in order to measure delay spread of a LOS environment with directional antennas [4], [6]. The large RMS delay spreads observed in LOS usually appear at off-boresight angles arising from multipath signal reflections and scattering in the environment, causing large delays with strong signals. Directional NLOS RMS delay spreads are for RX locations where obstructions blocked the clear optical LOS path from the TX. Table I shows the number of TX-RX location combinations where signal was measured, and the corresponding T-R separation distances for LOS and NLOS environments at 28 GHz and 73 GHz.

Table III provides the directional mean RMS delay spreads and standard deviations observed at 28 GHz and 73 GHz in LOS and NLOS environments. The mean LOS RMS delay spreads measured at 28 GHz and 73 GHz were 28.8 ns and 13.9 ns, respectively, and are both larger than their corresponding mean NLOS RMS delay spreads of 17.4 ns and 11.1 ns, indicating that scattered energy is more prominent in LOS environments when looking in arbitrary directions. Fig. 1 displays that 90% of the measured RMS delay spreads occur within 80 ns and 38 ns in LOS environments at 28 GHz and 73 GHz, respectively, whereas 90% of measured RMS delay spreads in NLOS environments are within 39 ns and 25 ns at 28 GHz and 73 GHz, respectively. The larger LOS and NLOS RMS delay spreads at 28 GHz imply that reflections are stronger at 28 GHz and that diffuse scattering is more important for the propagation path at 73 GHz (this is also seen in Figs. 1 and 2, and Tables III and IV). The NLOS mean RMS delay spreads at 28 GHz and 73 GHz compare well with other mmWave RMS delay spreads that are typically lower than 20 ns [15], [16].

Large RMS delay spreads in LOS environments occur when the TX and RX antennas are not aligned on boresight. Proper beam pointing in mmWave systems can direct antennas to the strongest received power or smallest delay spread angle combinations between TX and RX antennas, effectively reducing RMS delay spread and resulting in an improved link budget [17]. Fig. 2 shows the RMS delay spread CDFs from the unique pointing angles (in both azimuth and elevation lane) at both the TX and RX that resulted in the strongest received power for each TX-RX location combination in LOS and NLOS environments. Fig. 2 reveals that directional RMS delay spreads when only considering the single strongest beam power for a TX-RX location combination, are less than 2 ns at 28 and 73 GHz, thus illustrating that the angles with the strongest received power correspond to the LOS boresight link. Table IV shows the directional single strongest beam LOS and NLOS mean RMS delay spreads and standard deviations at 28 GHz and 73 GHz. Improvements for the mean RMS delay spread when considering the single strongest beam powers compared to arbitrary beams, are observed in LOS environments, where the strongest path is always the boresight-to-boresight link between the TX and RX antennas, compared to any arbitrary direction. At 28 GHz, the single strongest

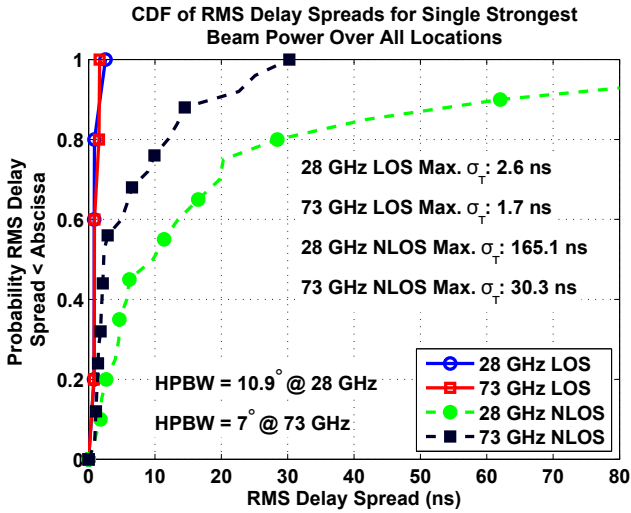


Fig. 2: 28 GHz and 73 GHz directional RMS delay spread CDFs for the single strongest beam power² over all TX-RX location combinations using directional antennas (HPBW of 10.9° at 28 GHz and 7° at 73 GHz) in New York City in LOS and NLOS environments. Table I shows the corresponding T-R separation distances and measured locations. Table IV show the mean RMS delay spreads and standard deviations for the strongest single beam power over all locations³.

TABLE IV: LOS and NLOS mean RMS delay spreads and standard deviations for the strongest single beam power over all locations in New York City at 28 GHz and 73 GHz.

Strongest Single Beam Power RMS Delay Spread Over All Locations with Signal ²	LOS		NLOS	
	μ (ns)	σ (ns)	μ (ns)	σ (ns)
28 GHz (10.9° HPBW)	1.19 ³	0.76 ³	25.7	40.2
73 GHz (7° HPBW)	1.16	0.42	7.1	8.3

beam power mean RMS delay spread over all locations for NLOS is larger than for the arbitrary pointing angle case due to a large number of angles at 28 GHz with low RMS delay spreads, but when comparing Fig. 1 and Fig. 2, the trend of the CDF curve is relatively consistent up until the 70% mark. The higher 28 GHz delay spread is likely due to the experimental design of the 28 GHz measurements that did not seek out the stongest beam pointing angles at the TX and RX. With beam searching and beamforming algorithms, directional RMS delay spreads for the strongest single beam powers will reduce ISI, thereby significantly improving connectivity and data throughput in a LOS mmWave network [17].

²Strongest single beam power refers to the unique antenna pointing angles in the azimuth and elevation plane at both the TX and RX for each location combination that resulted in the strongest received power.

³Mean and standard deviation values are calculated for five of six LOS locations at 28 GHz. The sixth LOS location had a larger than normal RMS delay spread (153.5 ns) as the TX and RX antennas were not properly aligned on boresight for that T-R separation distance, due to not searching for the best pointing angles.

III. DISTANCE EXTENSION USING BEAM COMBINING

Beamforming and beam combining techniques will be feasible for mmWave wireless and will improve link margin at cell edges, or equivalently offer, increased cell coverage beyond the estimated 200 m cell radius [17]. We quantify the distance extension by introducing a new concept of a *distance extension exponent* (DEE), used to determine distance extension curves as a function of T-R separation distance by combining beams at the mobile handset.

Enabling distance extension through beam combining can be understood by considering two mean path losses $PL_{(1 \text{ beam})}(d_1)$ at distance d_1 for the single best beam and $PL_{(\text{multibeam})}(d_2)$ at distance d_2 for combining beams. Both path loss values are equivalent such that:

$$PL_{(1 \text{ beam})}(d_1) = PL_{(\text{multibeam})}(d_2) \quad (4)$$

Below, the DEE derivation is based on a close-in free space reference distance, $d_0 = 1$ m, as this provides a standard for all measurements and models standardized to a 1 m reference. The distance extension exponent can be determined by solving for d_2 in terms of d_1 , Eq. (4) remains valid for all (d_1, d_2) pairs. Given the two path loss exponents (PLE) n_1 (single best beam) and n_2 (multibeam) (with respect to a free space reference distance $d_0 = 1$ m), we can estimate $PL_{(1 \text{ beam})}(d_1)$ and $PL_{(\text{multibeam})}(d_2)$ using the close-in free space reference distance path loss models in the following way:

$$PL_{(1 \text{ beam})}(d_1) = PL_{\text{FS}}(d_0) + 10n_1 \log_{10} \left(\frac{d_1}{d_0} \right) \quad (5)$$

$$PL_{(\text{multibeam})}(d_2) = PL_{\text{FS}}(d_0) + 10n_2 \log_{10} \left(\frac{d_2}{d_0} \right) \quad (6)$$

where $PL_{\text{FS}}(d_0)$ is the free space path loss at the standardized reference distance $d_0 = 1$ m. After substituting (5) and (6) into (4), we obtain the relationship between d_2 and d_1 such that (4) remains valid:

$$(d_2) = (d_1)^{\frac{n_1}{n_2}}, \quad (n_1 \geq n_2, \text{ always}) \quad (7)$$

where $\frac{n_1}{n_2}$ defines the DEE. Table V provides empirical values for the DEE under different beam combining scenarios, where n_1 describes the PLE under the single best beam, and n_2 describes the PLE for coherently or non-coherently combining multiple beams [17]. Coherent combining is done by summing the square root of strongest received powers, in Volts and squaring the sum, resulting in Watts, whereas non-coherent combining simply adds the strongest received powers together in Watts, and both methods are performed during post-detection [3], [17]. For example, a maximum cell radius of 200 m for the single best beam can be extended to 448 m when combining the four best beams coherently (DEE = 1.152), extending the coverage distance by a factor of 2.24 as seen in Eq. (10).

The effective *distance extension factor* (DEF) for a given T-R separation distance d_1 (PLE = n_1) when combining the

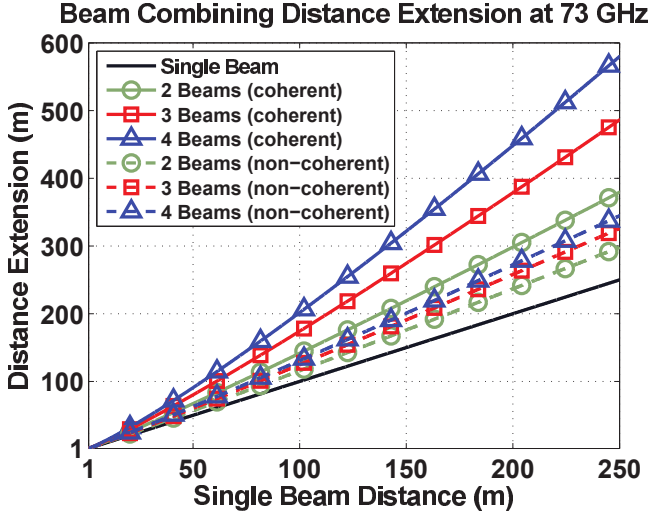


Fig. 3: Beam combining distance extension curves at 73 GHz for coherently and non-coherently combining the best beams compared to the single best beam. 28 GHz beam combining distance extension follows the same trend as the 73 GHz data.

best four beams compared to the single best beam, that results in d_2 (PLE = n_2) is computed as follows:

$$\text{DEF}(d_1, d_2) = \frac{d_2 - d_1}{d_1} + 1 \quad (8)$$

or equivalently using the DEE:

$$\text{DEF}(d_1, \text{DEE}) = \left[d_1^{(\text{DEE}-1)} \right] \quad (9)$$

$$\text{DEF}(200, 1.152) = \left[200^{(1.152-1)} \right] = 2.24 \quad (10)$$

The DEE can be used to determine the increased distance for a user experiencing the same path loss for beam combining compared to the single best beam. Fig. 3 displays the distance extension for coherently and non-coherently combining the best beams compared to the single best beam at 73 GHz. The 28 GHz distance extension curves follow the same trend as shown in Table V. The use of a 1 m free space reference distance allows a standard propagation model to be used and allows such comparisons in system design.

IV. 3-D OMNIDIRECTIONAL RMS DELAY SPREADS

A. Recovering Omnidirectional RMS Delay Spreads

Omnidirectional PDPs were recovered at a majority of the measured RX locations from the directional measurements using a MATLAB-based 3-D ray-tracing package developed at NYU to emulate electromagnetic propagation, and to predict absolute time delays of propagating MPCs. Table VI shows the number of locations where omnidirectional PDPs were synthesized compared to the total number of measured locations, as not all locations were able to be synthesized since the database did not agree with our observations. An $800 \times 800 \text{ m}^2$ area was modeled in Google SketchUp, allowing 3-D

TABLE V: NLOS beam combining distance extension exponents (DEE) when considering the combination of the strongest beams compared to the single strongest beam and the corresponding PLEs with respect to a 1 m free space reference distance d_0 . A comparison in distance extension is also given for a path loss observed at a distance of 200 m for the single best beam and the distance extension when combining the best beams for which the same path loss would be observed.

Beam Combining PLE and Distance Extension Exponent ($d_0 = 1 \text{ m}$)							
Freq.		PLE (Over all angles) = 4.556					
28 GHz	10.9° HPBW	Coherent			Non-Coherent		
	Beams	PLE	DEE	d_2 if $d_1 = 200 \text{ m}$	PLE	DEE	d_2 if $d_1 = 200 \text{ m}$
	1	3.812	-	296 m	3.812	-	238 m
	2	3.548	1.074	376 m	3.692	1.033	261 m
	3	3.406	1.119	450 m	3.631	1.050	278 m
4	3.307	1.153		3.591	1.062		
73 GHz		PLE (Over all angles) = 4.687					
	7° HPBW	Coherent			Non-Coherent		
	Beams	PLE	DEE	d_2 if $d_1 = 200 \text{ m}$	PLE	DEE	d_2 if $d_1 = 200 \text{ m}$
	1	3.728	-	300 m	3.728	-	237 m
	2	3.466	1.076	380 m	3.613	1.032	258 m
3	3.327	1.121	448 m	3.557	1.048	272 m	
4	3.235	1.152		3.523	1.058		

environment-specific modeling with an accuracy of 5 m. Fig. 4 shows a typical ray-traced synthesized RX location where viable propagation paths are shown in red. The corresponding measured power azimuth spectrum is shown in Fig. 5 along with the ray-tracing predictions for the strongest angles of arrival [9]. Our ray-tracer predicted up to four strongest measured angles at each RX location with an accuracy of $\pm 20^\circ$, which was enough to estimate the absolute propagating time delays of the first arriving multipath components at each of the strongest measured angles. We note the ray-tracer was unable to predict angles that received weakly scattered energy as a result of the coarseness of the database used.

We synthesized absolute timing omnidirectional PDPs using the ray-tracing predictions with the measured data. The PDPs corresponding to the strongest measured azimuth and elevation angles were matched up with the corresponding shortest predicted absolute propagation distances resulting from the ray-tracing simulations. The excess delay PDPs from the strongest measured angles were then superimposed upon an absolute propagation time delay axis, where each PDP was appropriately shifted and added in time using the ray-tracing predicted absolute propagation time delay (obtained from dividing the predicted distance by the speed of light in free space) [9]. The strongest multipath components propagating from TX to RX were assumed to follow specular reflection paths and result in prominent angles, which could be simulated in the ray-tracing environment using the ‘‘Law of Reflection’’, a reasonable assumption in order to pair up strong measured angles and ray-tracing predictions. The resulting synthesized 3-D omnidirectional PDPs for measured RX locations were subsequently analyzed to extract the RMS delay spreads [5].

TABLE VI: Number of locations where omnidirectional PDPs were synthesized via ray-tracing.

	28 GHz	73 GHz
LOS locations synthesized for omnidirectional PDPs	3 out of 6	5 out of 5
NLOS locations synthesized for omnidirectional PDPs	13 out of 20	19 out of 25

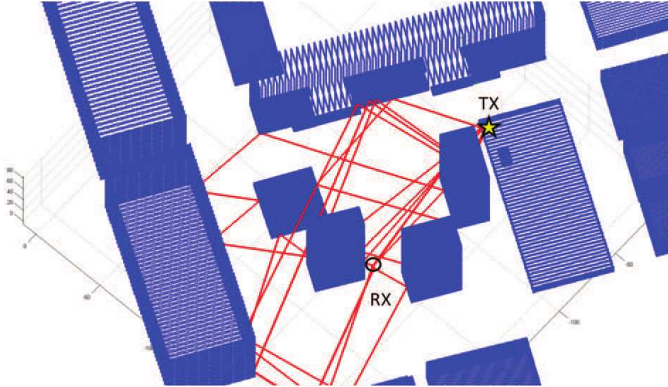


Fig. 4: A 3-Dimensional view of the Downtown Manhattan area obtained from the MATLAB-based 3-D ray-tracer. The rays which leave the TX and successfully arrive at the measured RX are shown in red, and represent multipath signal trajectories in a dense UMi. The TX was located on the rooftop of the Coles Sports Center 7 m above ground (yellow star), and the RX was located 113 m away, 1.5 m above ground (black circle) [9].

B. Millimeter-Wave Omnidirectional RMS Delay Spreads

Fig. 6 shows the 28 GHz and 73 GHz omnidirectional RMS delay spreads as a function of T-R separation distance in both LOS and NLOS environments, obtained from absolute timing omnidirectional PDPs. The mean LOS RMS delay spreads were 46.6 ns and 14.6 ns at 28 GHz and 73 GHz, respectively, and the corresponding NLOS values were 40.9 ns and 45.7 ns. These values depend significantly on the ray-tracing simulation results, required to recover the omnidirectional profiles. We also note that there are only three locations with synthesized omnidirectional RMS delay spreads for the 28 GHz LOS case. We again note that the 28 GHz measurements did not search for the angles that resulted in the strongest received power and did not measure all locations with antennas aligned on bore-sight. The RMS delay spread appears to slightly decrease as the T-R separation distance increases, where MPCs experience more reflections to arrive at the receiver. Finally, the 73 GHz mean omnidirectional NLOS RMS delay spreads are slightly larger than at 28 GHz, indicating that the received energy is more spread out in time, implying a more pronounced diffuse scattering effect at 73 GHz.

Fig. 7 shows the LOS and NLOS CDFs for the 28 GHz and 73 GHz omnidirectional RMS delay spreads. We observe that 50% of all RMS delay spreads lie below 25 ns at both 28 GHz and 73 GHz, and that 90% of all RMS delay spreads lie below 80 ns and 89 ns at 28 GHz and 73 GHz, respectively,

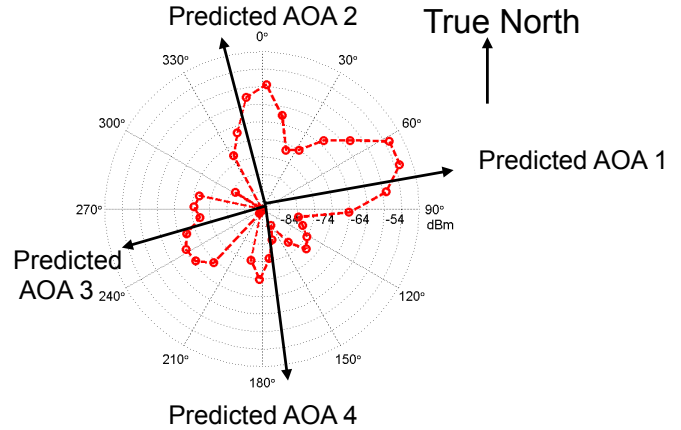


Fig. 5: Measured azimuthal distribution of total received power (dBm units), also referred to as a polar plot, showing the predicted AOAs (black arrows) using 3-D ray-tracing at the measured Manhattan RX location shown in Fig. 4. The center of the plot corresponds to the RX location. The RX and TX antennas both had 24.5 dBi of gain with 10.9° (in azimuth) and 8.6° (in elevation) 3 dB beamwidths, and the RX azimuth 0° mark points to the True North bearing direction [9].

TABLE VII: Mean and standard deviation of the 28 GHz and 73 GHz omnidirectional RMS delay spreads obtained from absolute timing PDPs in LOS and NLOS environments in Downtown Manhattan.

Omni. RMS Delay Spread	Frequency	LOS		NLOS	
		μ (ns)	σ (ns)	μ (ns)	σ (ns)
	28 GHz	46.6	39.7	40.9	57.0
	73 GHz	14.6	7.9	45.7	35.5

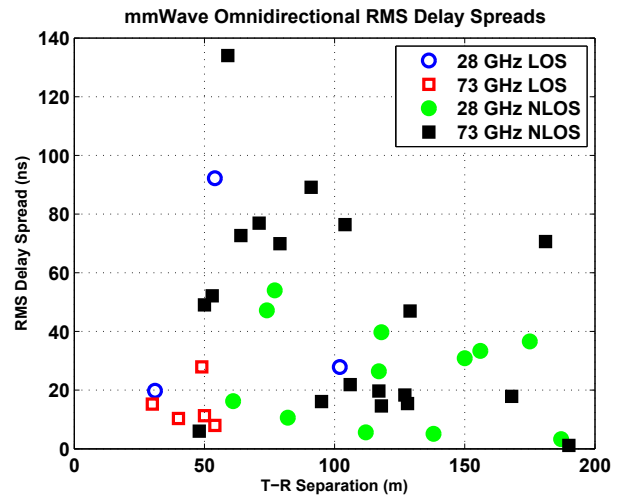


Fig. 6: Omnidirectional RMS delay spreads as a function of T-R separation distance obtained from synthesized absolute timing PDPs measured at 28 GHz and 73 GHz for LOS and NLOS channels in Downtown Manhattan, a dense UMi environment.

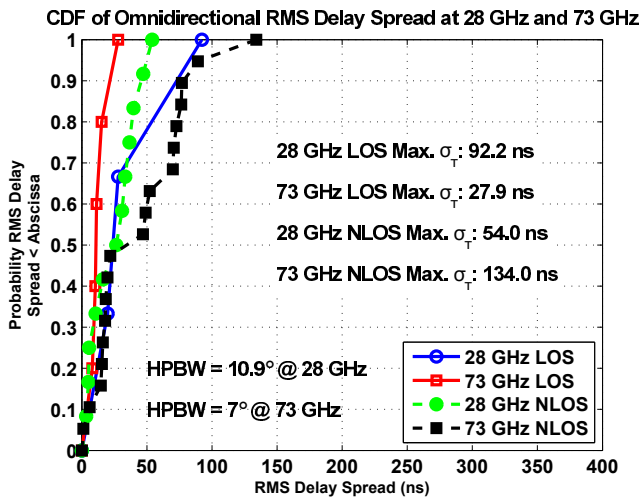


Fig. 7: CDFs of the omnidirectional RMS delay spreads obtained from synthesized absolute timing PDPs measured at 28 GHz and 73 GHz in LOS and NLOS environments in Downtown Manhattan, a dense UMi environment.

illustrating more diffuse scattering at 73 GHz, as the received energy is more spread out in time delay.

V. CONCLUSION

This paper presented directional and omnidirectional RMS delay spread statistics obtained from outdoor mmWave UWB propagation measurements using highly directional steerable horn antennas, and presented a new system design parameter. Distance extension with beam combining using a *distance extension exponent*, is useful in performing system-wide simulations. The DEE is made possible through the use of a 1 m free space reference distance for all LOS and NLOS path loss models, as described in [2]. Directional measurements over all unique pointing angles resulted in mean RMS delay spreads of 28.8 ns and 13.9 ns in LOS at 28 GHz and 73 GHz, respectively, as seen in Fig. 1 and Table III. The directional mean RMS delay spreads were 17.4 ns and 11.1 ns in NLOS environments at 28 GHz and 73 GHz, respectively, showing that 28 GHz has larger RMS delay spread than 73 GHz. Measured NLOS directional mean RMS delay spreads at angles with the strongest received power are 25.7 ns and 7.1 ns at 28 GHz and 73 GHz, respectively, a great reduction over NLOS omnidirectional RMS delay spreads as seen in Table VII where means of 40.9 ns and 45.7 ns were measured, respectively. The mean RMS delay spreads found at 28 GHz and 73 GHz in NLOS environments compare well with typical RMS delay spreads found at 59 GHz that are at or lower than 20 ns [15], [16]. Future mmWave coverage distance can also be extended significantly through beam combining, by a factor of more than 2.2 from 200 m when combining the four strongest beams over the single best beam at 73 GHz in a NLOS environment using a DEE. The synthesized omnidirectional RMS delay spreads are much larger than at arbitrary pointing angles for both LOS and NLOS, indicating that directional mmWave systems will be more useful for

avoiding ISI and thus improving signal quality and throughput. These results illustrate that mmWave UWB communications systems can be exploited with directional antennas at the TX and RX to achieve greater system performance.

REFERENCES

- [1] Z. Pi and F. Khan, "An introduction to millimeter-wave mobile broadband systems," *IEEE Communications Magazine*, vol. 49, no. 6, pp. 101–107, June 2011.
- [2] T. S. Rappaport, R. W. Heath, Jr., R. C. Daniels, and J. N. Murdock, *Millimeter Wave Wireless Communications*. Pearson/Prentice Hall, 2015.
- [3] S. Sun and T. Rappaport, "Wideband mmwave channels: Implications for design and implementation of adaptive beam antennas," in *2014 IEEE MTT-S International Microwave Symposium (IMS)*, June 2014, pp. 1–4.
- [4] T. S. Rappaport, S. Sun, R. Mayzus, H. Zhao, Y. Azar, K. Wang, G. N. Wong, J. K. Schulz, M. Samimi, and F. Gutierrez, "Millimeter wave mobile communications for 5G cellular: It will work!" *IEEE Access*, vol. 1, pp. 335–349, 2013.
- [5] M. K. Samimi and T. S. Rappaport, "3-D statistical channel models for millimeter-wave outdoor mobile broadband communications," in *2015 IEEE International Conference on Communications (ICC)*, June 2015.
- [6] G. R. MacCartney, Jr. and T. S. Rappaport, "73 GHz millimeter wave propagation measurements for outdoor urban mobile and backhaul communications in New York City," in *2014 IEEE International Conference on Communications (ICC)*, June 2014, pp. 4862–4867.
- [7] T. S. Rappaport, E. Ben-Dor, J. N. Murdock, and Y. Qiao, "38 GHz and 60 GHz angle-dependent propagation for cellular & peer-to-peer wireless communications," in *2012 IEEE International Conference on Communications (ICC)*, June 2012, pp. 4568–4573.
- [8] G. R. MacCartney, Jr., M. K. Samimi, and T. S. Rappaport, "Omnidirectional path loss models from measurements recorded in New York City at 28 GHz and 73 GHz," in *2014 IEEE 25th International Symposium on Personal Indoor and Mobile Radio Communications (PIMRC)*, Sept. 2014.
- [9] M. K. Samimi and T. S. Rappaport, "Ultra-wideband statistical channel model for non line of sight millimeter-wave urban channels," in *2014 IEEE Global Telecommunications Conference (GLOBECOM 2014)*, Dec. 2014, pp. 8–12.
- [10] S. Hur, Y.-J. Cho, T. Kim, and J. Park, "Millimeter-wave channel modeling based on measurements in in-building, campus and urban environments at 28 GHz," *COST IC1004*, Sept 2014.
- [11] "WP5: Propagation, antennas and multi-antenna technique, channel modeling and characterization," in *MiWEBA Deliverable D5.1*, June 2014.
- [12] Y. Zahedi, R. Ngah, U. Chude-Onkonkwo, S. Nunoo, and M. Mokayef, "Modeling the RMS delay spread in time-varying UWB communication channels," in *2014 5th International Conference on Intelligent and Advanced Systems (ICIAS)*, June 2014, pp. 1–5.
- [13] X. Mao, Y. H. Lee, and B. C. Ng, "Wideband channel modelling in UHF band for urban area," in *2008 IEEE International Symposium on Wireless Communication Systems (ISWCS)*, Oct. 2008, pp. 240–244.
- [14] N. Moraitis, A. Kanatas, G. Pantos, and P. Constantinou, "Delay spread measurements and characterization in a special propagation environment for PCS microcells," in *The 13th IEEE International Symposium on Personal, Indoor and Mobile Radio Communications*, vol. 3, Sept. 2002, pp. 1190–1194.
- [15] G. Lovnes, J. Reis, and R. Raekken, "Channel sounding measurements at 59 GHz in city streets," in *1994 5th IEEE International Symposium on Personal, Indoor and Mobile Radio Communications. Wireless Networks - Catching the Mobile Future.*, vol. 2, Sept. 1994, pp. 496–500.
- [16] P. Smulders and L. Correia, "Characterisation of propagation in 60 GHz radio channels," *Electronics Communication Engineering Journal*, vol. 9, no. 2, pp. 73–80, Apr. 1997.
- [17] S. Sun, T. S. Rappaport, R. W. Heath, A. Nix, and S. Rangan, "Mimo for millimeter-wave wireless communications: beamforming, spatial multiplexing, or both?" *IEEE Communications Magazine*, vol. 52, no. 12, pp. 110–121, Dec. 2014.
- [18] T. S. Rappaport, J. N. Murdock, and F. Gutierrez, "State of the art in 60-GHz integrated circuits and systems for wireless communications," *Proceedings of the IEEE*, vol. 99, no. 8, pp. 1390–1436, Aug. 2011.